2.B X-Ray Conversion Measurements from High-Z Spherical Targets

Quantitative measurements of the x-ray emission from laser-produced plasmas have been a subject of considerable interest since the early 1970s.[1] With the fabrication of large, in some cases multibeam, high-power laser systems, much work has been performed on the analysis of x-ray emission from laser-produced plasmas of high-atomic-number materials.[2] Measurements of soft x-ray emission from the plasmas of high-Z materials, particularly Au targets, are not only of considerable interest for inertial confinement fusion applications but are also relevant to a number of potential applications of laser-produced x rays. For these reasons, there is a need for the quantitative understanding, through hydrodynamic and atomic physics numerical codes, of soft x-ray production from laser-irradiated solid targets. This is particularly the case for interaction experiments with high-power, short-wavelength laser radiation. Such experiments exhibit not only high overall coupling efficiency but also produce, for high-Z targets, greater soft x-ray emission. However, experiments to date have all been performed with planar targets, irradiated by single or nonuniform multiple-laser beams. A number of studies have been performed at Lawrence Livermore National Laboratory (LLNL) with the ARGUS[3] and NOVETTE[4] laser systems to compare the experimentally determined conversion efficiencies to x rays and those estimated from numerical simulations performed with the laser-fusion hydrodynamic code *LASNEX*. At low intensities ($<8\times10^{13}$ W/cm^2), the measured x-ray conversion efficiency[3] is lower than that predicted by *LASNEX*.

In a collaborative set of experiments between Los Alamos National Laboratory (LANL) and the Laboratory for Laser Energetics (LLE), the first detailed investigation of x-ray conversion from high-Z (Au) spherical targets was made during the summer of 1984.[5] This investigation used a symmetric (cubic) set of six UV beams from the 24-beam OMEGA laser system.[6] The primary motivation behind these investigations was the study of x-ray conversion in a nearly 1-D spherical experiment to determine if previously observed discrepancies still exist. To this aim, detailed measurements were made in one dimension of the energy flow, coronal plasma conditions, and emission characteristics of x rays. From these studies it was hoped to identify modifications to the *LASNEX* model required to correctly match experimental observables.

These studies were made with an extensive array of x-ray diagnostics, fielded jointly by LLE and LANL, including (a) a four-channel, absolutely calibrated x-ray diode spectrometer, (b) a 15-channel diode/scintillator-photomultiplier x-ray continuum emission spectrometer, (c) x-ray crystal and grazing incidence XUV spectrographs, (d) a time-resolved (streak) x-ray grating spectrograph, (e) a time-resolved (streak) curved x-ray crystal spectrograph (SPEAX), (f) x-ray pinhole camera and microscope imaging, and (g) time-resolved x-ray streak photography. In addition, coronal plasma conditions were monitored with plasma calorimeters, charged collectors, harmonic emission diodes, and spectrographic

measurements of the $\omega/2$ harmonic emission. In the experiments, six 351-nm beams of OMEGA irradiated Au-coated, solid CH targets with intensity range at two intensities, 4×10^{13} W/cm^2 and 4×10^{14} W/cm^2. For OMEGA irradiation conditions, a sharp transition occurs between the low- and high-intensity cases; in the latter case, short scale lengths produce higher coronal temperatures, a higher ionization state, and the consequential emission of M-line radiation. A detailed set of measurements were made with targets having various thicknesses of Au to investigate the progress of the ionization front, and the burn-through to the underlying low-Z material. All these experiments were performed with the six UV beams focused tangentially on spherical targets of 600-μm or 200-μm diameter, to provide the maximum level of irradiation uniformity with total energies of the order of 250 J in 600-ps (FWHM) pulses.

Absolute x-ray flux measurements were made with four calibrated soft x-ray diodes, each sampling separate regions of the x-ray emission between 0.1 and 1 kV through the use of a number of thin metallic and plastic filters. The overall x-ray conversion (~60%), shown in Fig. 22.7, indicates little apparent intensity dependence. At the lower

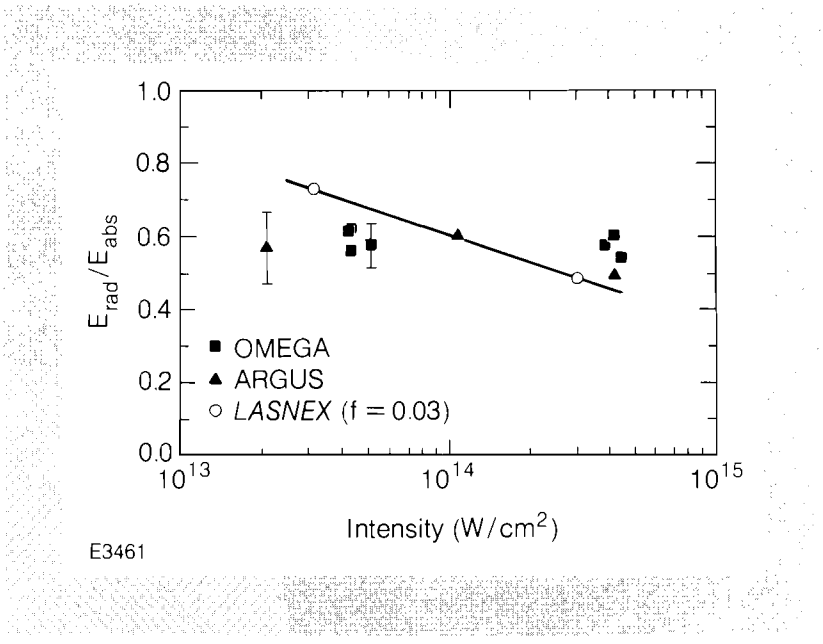

Fig. 22.7
X-ray conversion as a function of incident intensity.

intensity (~4×10^{13} W/cm^2), the conversion of the incident laser energy into x rays was 0.52, this value dropping to 0.44 at intensities of ~4×10^{14} W/cm^2. This observation is consistent with the previous planar target (ARGUS) data but deviates, particularly at low intensities, from the predictions of a flux-limited (f = 0.03) *LASNEX* model. This difference between simulations and experiment at low intensities requires further study; in a future series of measurements, x-ray conversion at lower intensities and at higher intensities in spherical geometry will be measured. In studies of the x-ray conversion as a function of the Au thickness, *LASNEX* in general predicted well the observed falloff in x-ray conversion for thin Au layers at both intensities. Experimental data are given in Fig. 22.8. As shown in Fig. 22.9, the falloff in x-ray conversion

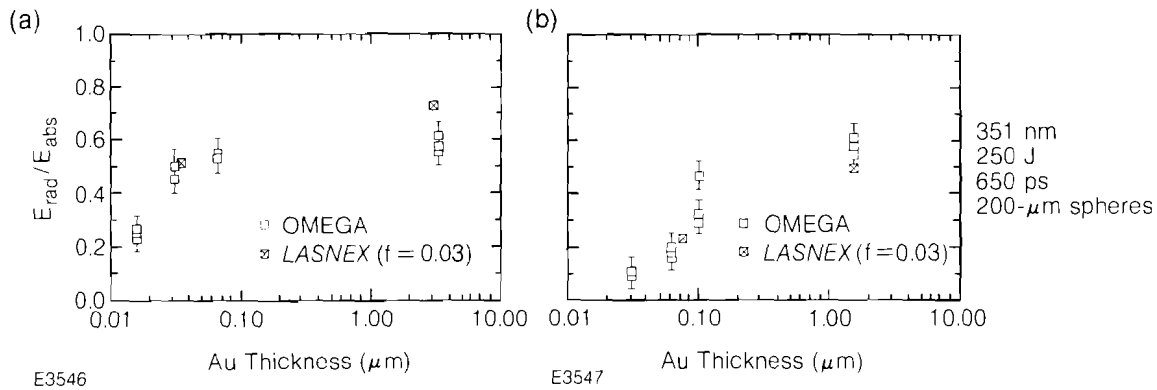

Fig. 22.8
Variation in x-ray conversion as a function of Au thickness for (a) 4×10^{14} W/cm^2 and (b) 4×10^{13} W/cm^2.

occurred at a thickness at which the conversion efficiency of half-harmonic emission increased by an order of magnitude, and where the x-ray bremsstrahlung yield from superthermal electrons, measured with the K-edge spectrometer, increased several fold. This indicates that under conditions where burn-through of the gold occurs during the laser pulse, the underdense scale length changes to permit the onset of the 2 ω_p instability at $n_c/4$, resulting in an increase in $\omega/2$ emission and superthermal electrons.[7]

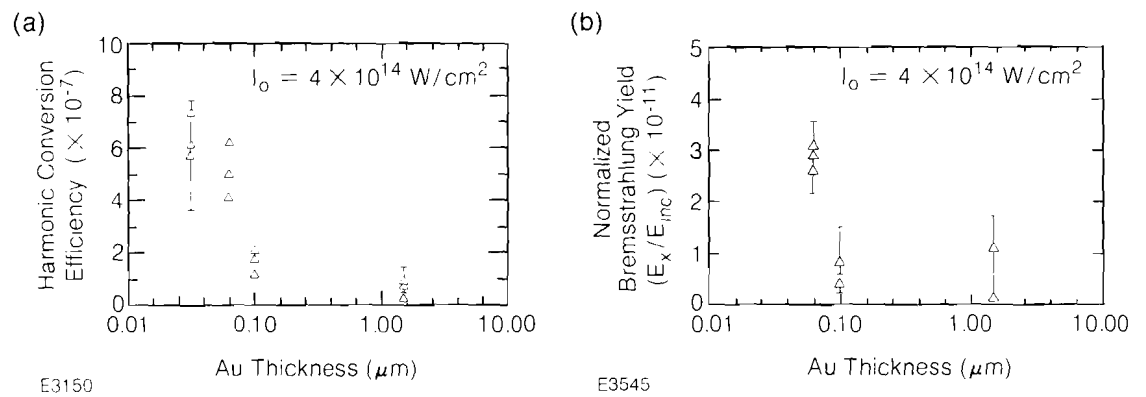

Fig. 22.9
Change in the level of $\omega/2$ harmonic emission (a), and superhot bremsstrahlung x-ray emission (b), as the thickness of Au is decreased below the burn-through thickness.

A parametric study of M-line emission from Au targets was made using time-integrated and time-resolved spectrographic instrumentations. At the higher intensity of 4×10^{14} W/cm^2, *LASNEX* predicts, as shown in Fig. 22.10(a), the onset of strong M-line emission due to the creation of a higher temperature. Experimentally, the *LASNEX* prediction was confirmed, as shown in Figs. 22.10(b) and 22.10(c). These figures show the lack of any strong M-line emission at 4×10^{13} W/cm^2 and its strong appearance in the 5- to 6-Å region at 4×10^{14} W/cm^2. At the higher intensities, the onset of M-line emission was also found to be strongly dependent on the thickness of Au. For the smallest thicknesses used (0.06 μm), the level of M-line emission was small.

Fig. 22.10
Onset of strong M-line emission in going from 4×10^{13} W/cm^2 as predicted by LASNEX *(a) and as found in experiment at 4×10^{13} W/cm^2 (b) and 4×10^{14} W/cm^2 (c).*

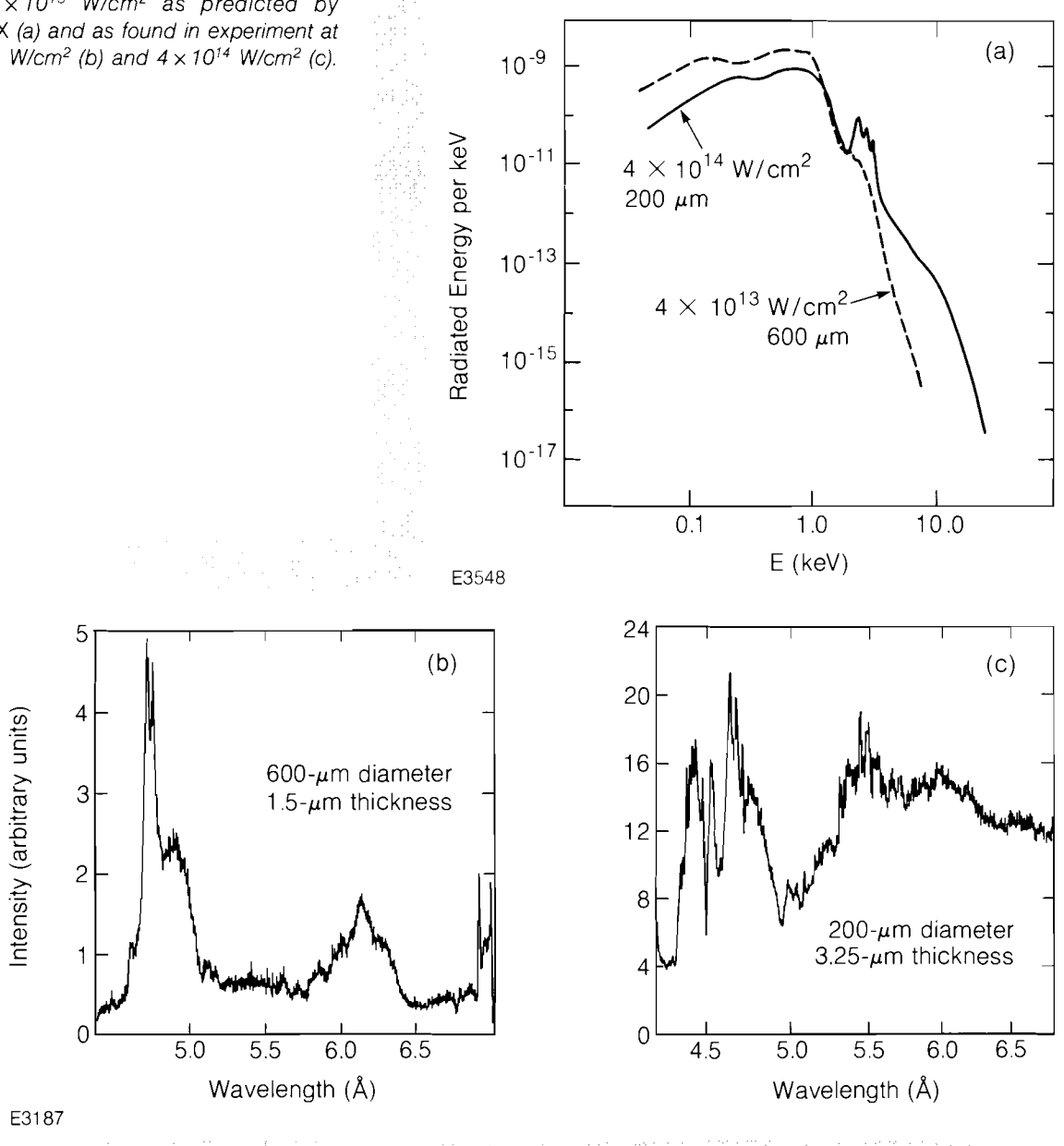

Time-resolved x-ray spectral measurements were made with two devices, a transmission-grating streak spectrograph,[8] sensitive in the 1- to 30-Å region, and an elliptical crystal streak spectrograph,[9] sensitive in the 5.2- to 7.1-Å region. The former instrument had a broad spectral range but limited resolution ($\lambda/\Delta\lambda \sim 100$), while the latter had high resolution ($\lambda/\Delta\lambda \sim 1000$) but a limited spectral range, centrally located in the band of M-lines. While the M-line emission appears as a broadband centered in the 5- to 6-Å region in the transmission-grating spectrograph, details of the M-lines can be seen from the crystal streak spectrograph. Detailed convolution of data such as shown in Fig. 22.11 can render considerable information about the temporal evolution of the

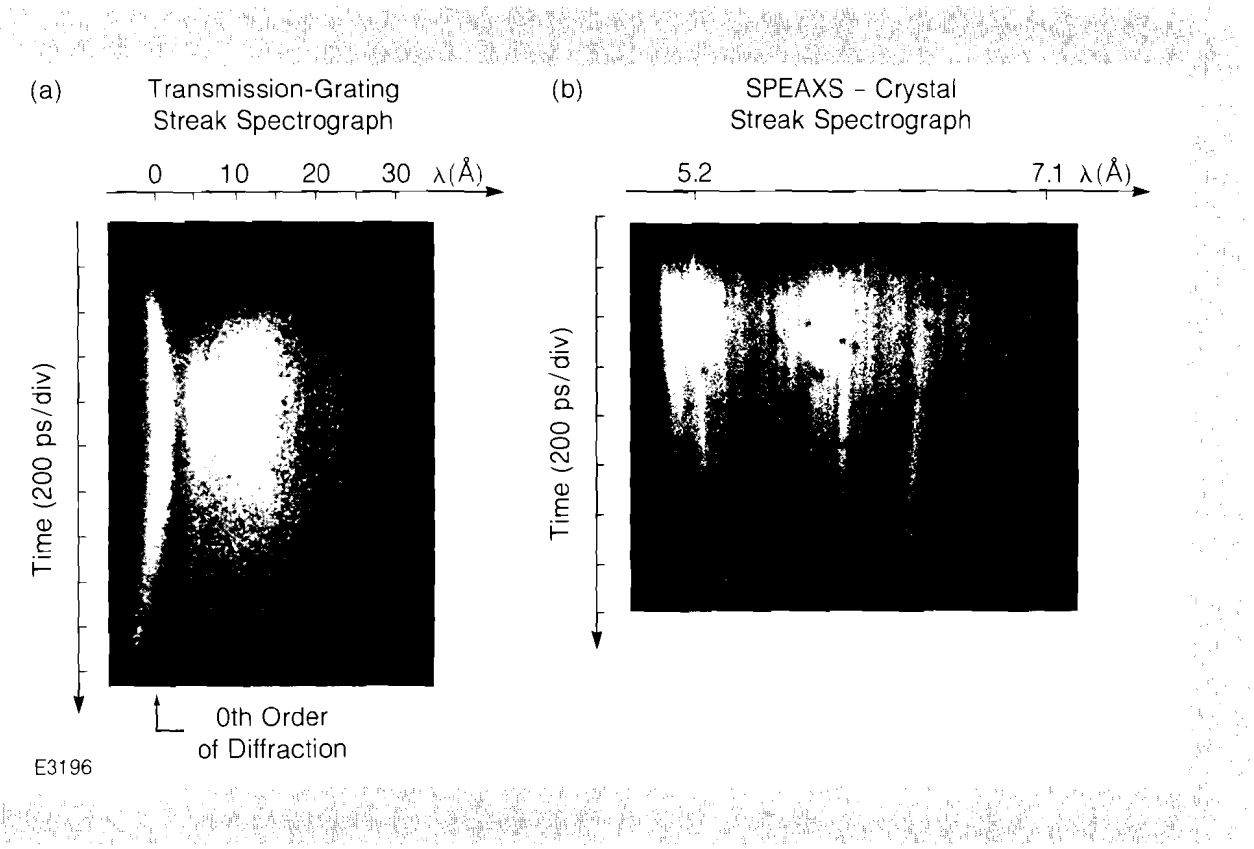

Fig. 22.11
Typical time-resolved spectra obtained from Au targets and the transmission-grating streak spectrograph (a), and the crystal streak spectrograph, SPEAXS (b).

M-line emission. Figure 22.12(a) shows, for example, the duration of the M-line emission from 4.8–6.9 Å, deduced from the transmission-grating spectrograph, for the case of a 0.062-μm, thick-coated Au target at high intensity. The duration of the M-line emission is considerably shorter than the 600-ps duration (FWHM) of the laser pulse. This should be compared with the *LASNEX* prediction of the duration of the M-line emission under these conditions, shown in Fig. 22.12(b). There is reasonably close agreement between simulation and experiment. In general, *LASNEX* models well the duration of the M-line emission under various irradiation conditions, with the exception that in the case of very thin Au target layers, at high intensities, the duration of the M-line emission is truncated less sharply than the code would predict. This may well be a consequence of the effects of irradiation nonuniformities on the surface of the target, a subject which will be discussed in more detail.

The streak x-ray crystal spectrograph, with its high resolution, can provide detailed information on the time evolution of M-lines. Figure 22.13 shows time-resolved spectra of the M-line emission for targets irradiated at high intensity (4×10^{14} W/cm^2) for different thicknesses of Au-coated CH targets. The duration of the individual M-lines is reduced as the thickness of Au is reduced. The wavelength of these specific M-lines, not well known at present, is calibrated by fiducial Si lines emanating from portions of the glass stalk used to support the target. Reduction of this data can render extremely detailed information on the time history of all M-lines observed.

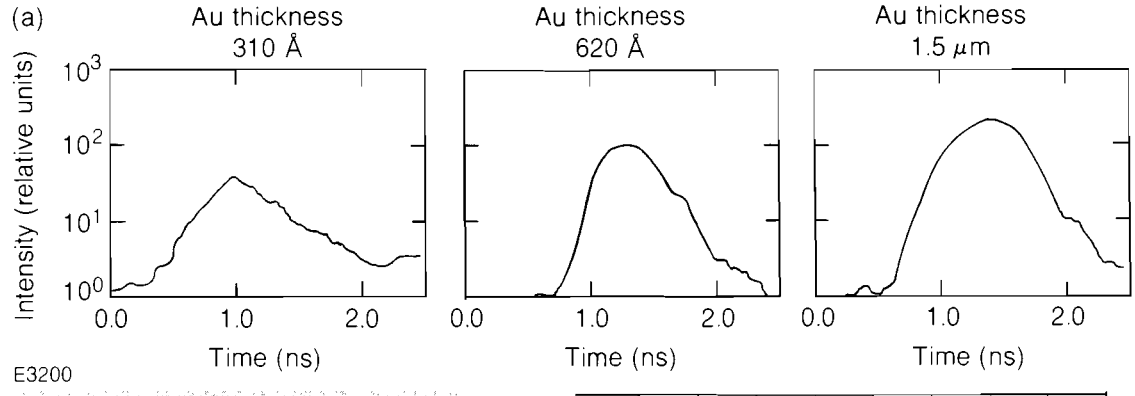

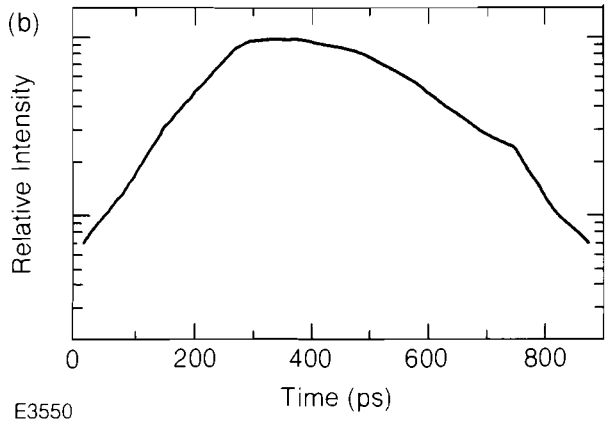

Fig. 22.12
Time history of M-line emission deduced from x-ray grating streak spectrograph (a), for a 620-Å-thick Au layer, irradiated at 4×10^{14} W/cm^2, compared to the prediction from LASNEX *(b).*

Fig. 22.13
Details of the temporal evolution of the M-line emission, produced by the SPEAXS instrument, for various thicknesses of Au, irradiated at 4×10^{14} W/cm^2. Fiducial Si lines, emanating from portions of the glass stalk evaporated by the laser, are also observable.

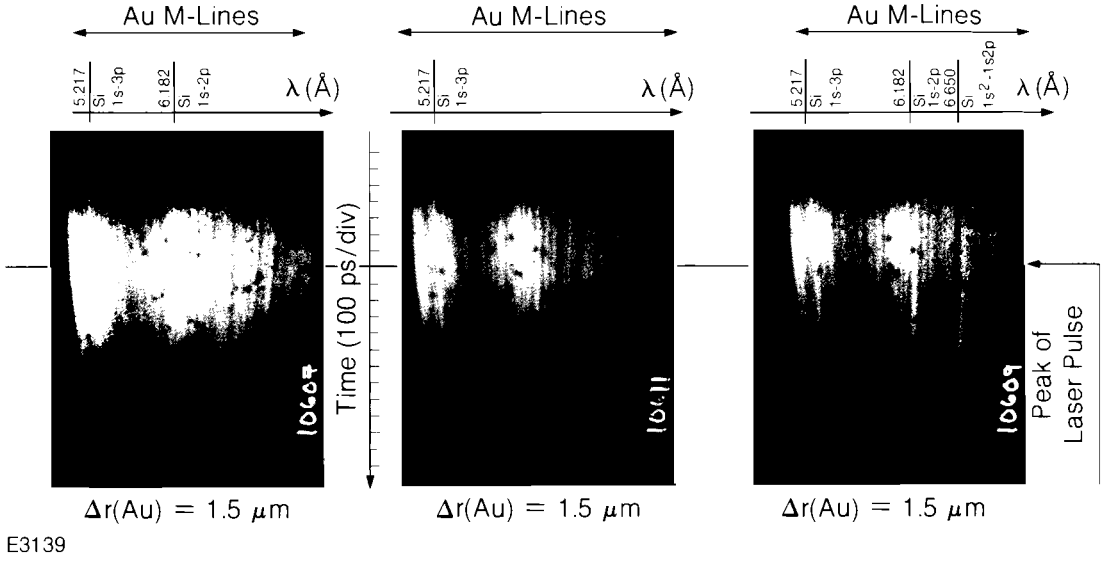

Detailed diagnosis of x-ray images in these experiments was performed to evaluate the level to which uniform irradiation of the target could be depended upon, and to identify nonuniformities in the surface x-ray emission of the target. Several different instruments were used. Figure 22.14 shows typical x-ray images of the target obtained with three different instruments – a pinhole camera filter combination selecting x-ray emission in the sub-keV range, a second pinhole camera/filter system producing images of 1.0-keV x-ray emission, and a Kirkpatrick-Baez microscope, which produces x-ray images in the 3-keV x-ray emission. Analysis of these x-ray images, as for example

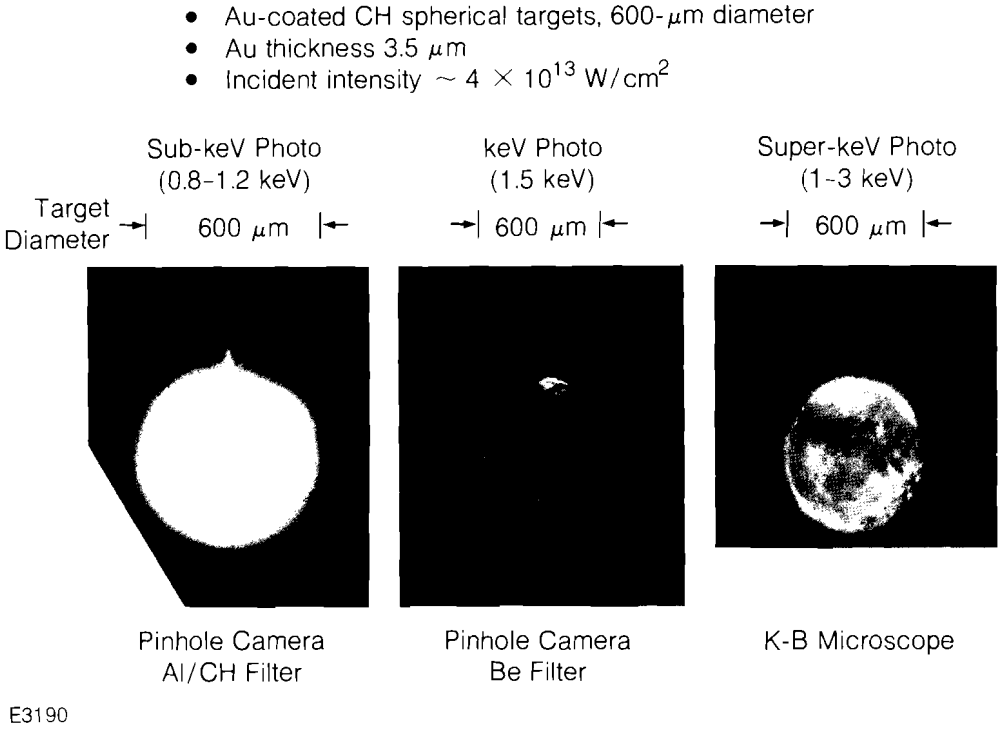

Fig. 22.14
X-ray analysis in different x-ray regions, detailed with two pinhole cameras and a Kirkpatrick-Baez microscope.

shown in Fig. 22.15(a), indicates that the variation in x-ray emission across the surface of the target in regions of the image where limb brightening is not a factor can be at least a factor of 2. The level of irradiation uniformity incident on the target, for six beam irradiation conditions, is shown in Fig. 22.15(b).[10] Disregarding the small intense hot spots in the irradiation distribution, it can be seen that the overall variation in intensity in long spatial frequencies is approximately a factor of 2; qualitatively, this is comparable to the x-ray photographic data. Assuming the same level of uniformity presently existing in each individual beam, it is expected that with 24-beam irradiation at the same irradiation and focusing conditions, the overall level of irradiation uniformity on the surface of the sphere will improve by at least a factor of 6.

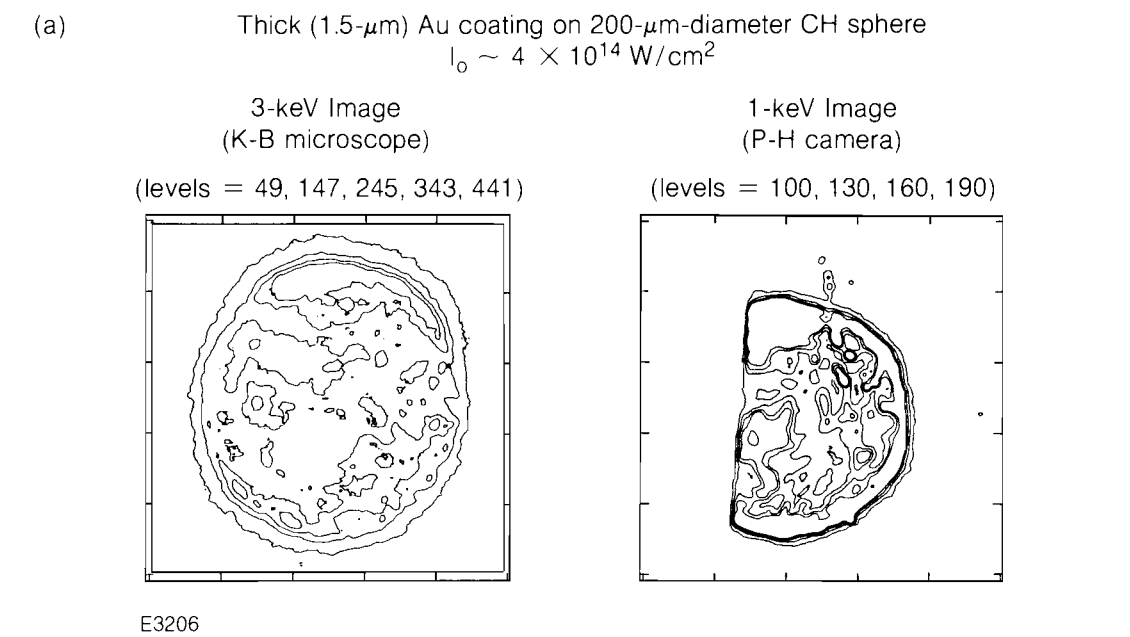

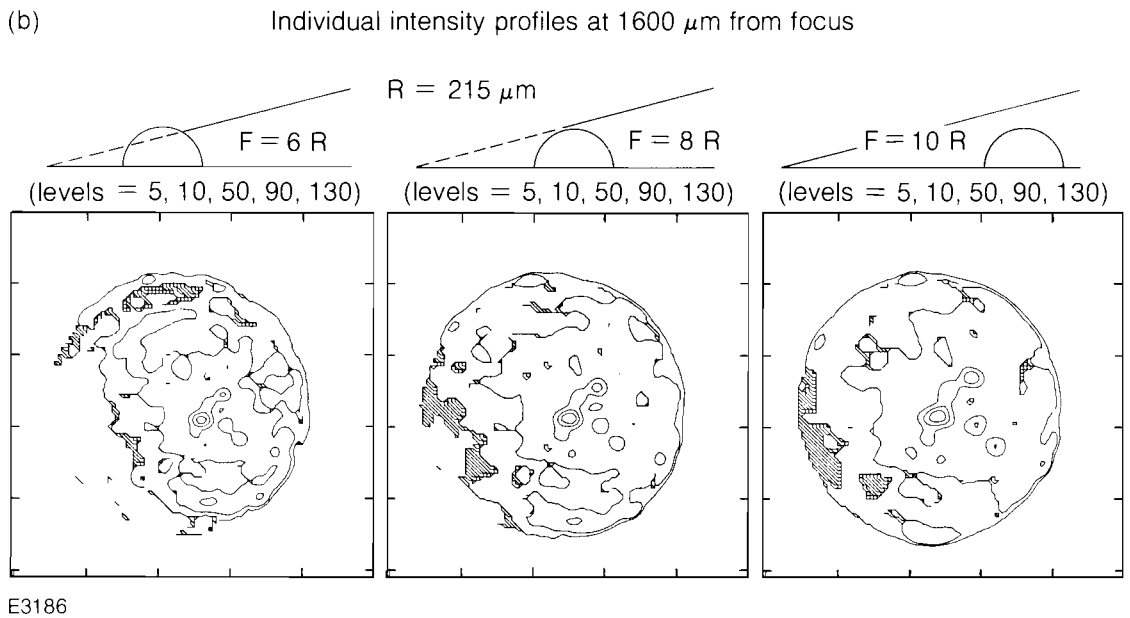

Fig. 22.15
Nonuniformities evident in x-ray emission on the surface of the target (a), compared to estimated irradiation nonuniformities deduced from a detailed knowledge of the intensity distributions of each beam, mapped onto the surface of a sphere (b).

Time-resolved photographic studies of the emission from the target were made with a streak x-ray pinhole camera system. Some typical data, taken at low irradiation conditions (4×10^{13} W/cm^2), are shown in Fig. 22.16. For both thick and thin layers of gold, spatial structure is clearly evident in the x-ray emission. The level to which this spatial structure in the x-ray emission alters the 1-D description used in the *LASNEX* simulation is under detailed study.

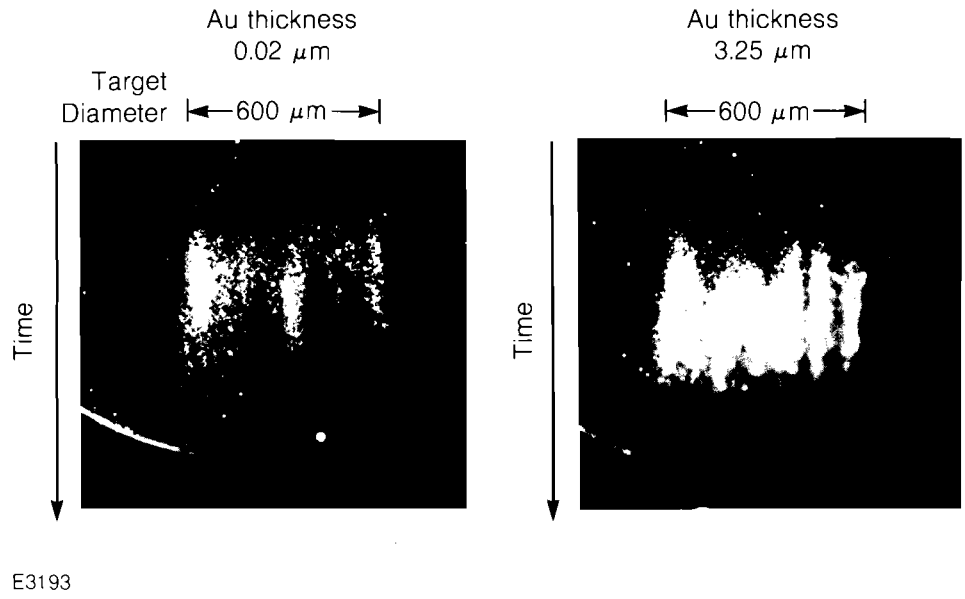

Fig. 22.16
Time-resolved x-ray photography of Au-coated targets at an intensity of 4×10^{13} W/cm^2.

In summary, this comprehensive characterization of x-ray conversion from spherical high-Z (Au) targets with short-wavelength irradiation has produced much interesting information. Detailed measurements of the dependence of the x-ray conversion efficiency on laser irradiance has confirmed a previously observed intensity dependence, which is smaller than that predicted by the *LASNEX* hydrodynamic code. The deployment of a large array of time-resolved, space-resolved, and time-integrated x-ray instrumentation has rendered an extensive investigation of the Au M-line emission with high spectral, spatial, and temporal resolution. The data from several diagnostics specifically deployed to characterize coronal plasma conditions compare well to code predictions. Finally, although there is, in general, close agreement between the experimental data and the 1-D *LASNEX* predictions, the effects of irradiation nonuniformities across the surface of the target, produced with only six-beam irradiation conditions, cannot be ignored. The level of irradiation uniformity has been assessed from detailed knowledge of beam characteristics and through x-ray microscopy. It is anticipated that in future experiments, performed with 24 beams, the effects of microscopic nonuniformities across the surface of the target will be reduced compared to the six-beam experiments.

ACKNOWLEDGMENT

This work was supported by the U.S. Department of Energy Office of Inertial Fusion under agreement number DE-FC08-85DP40200 and in part by Los Alamos National Laboratory under subcontract 9-XR4-P1019-1, effective 1 May 1984.

REFERENCES

1. D. J. Nagel *et al.*, *Phys. Rev. Lett.* **33**, 743 (1974).
2. B. Yaakobi, T. Boehly, P. Bourke, Y. Conturie, R. S. Craxton, J. Delettrez, J. M. Forsyth, R. D. Frankel, L. M. Goldman, R. L. McCrory, M. C. Richardson, W. Seka, D. Shvarts, and J. M. Soures, *Opt. Comm.* **39**, 175 (1981).
3. W. C. Mead *et al., Phys. Rev. Lett.* **47**, 1289 (1981).
4. R. L. Kauffman *et al., Bull. Am. Phys. Soc.* **29**, 1183, paper 1R1 (1984).
5. P. D. Goldstone, R. H. Day, G. Eden, F. Ameduri, W. C. Mead, S. R. Goldman, M. C. Richardson, R. L. Keck, W. Seka, G. Pien, J. M. Soures, and R. L. McCrory, *Bull. Am. Phys. Soc.* **29**, 1318, paper 6E5 (1984); R. S. Marjoribanks, G. Stradling, M. C. Richardson, A. Hauer, O. Barnouin, B. Yaakobi, S. A. Letzring, and P. D. Goldstone, *ibid.* **29**, 1318, paper 6E6 (1984); S. A. Letzring, M. C. Richardson, P. D. Goldstone, G. Gregory, and G. Eden, *ibid.* **29**, 1318, paper 6E7 (1984); S. R. Goldman, W. C. Mead, P. D. Goldstone, and M. C. Richardson, *ibid.* **29**, 1319, paper 6E8 (1984).
6. LLE Review **17**, 3 (1983); J. M. Soures, R. J. Hutchison, S. D. Jacobs, L. D. Lund, R. L. McCrory, and M. C. Richardson, in Proceedings of the 10th Symposium on Fusion Engineering, Philadelphia, 1983.
7. W. Seka, B. B. Afeyan, R. Boni, L. M. Goldman, R. W. Short, K. Tanaka, and T. W. Johnson (submitted for publication).
8. M. C. Richardson, R. S. Marjoribanks, S. A. Letzring, J. M. Forsyth, and D. M. Villeneuve, *IEEE J. Quantum Electron.* **QE-19**, 1861 (1983).
9. B. L. Henke and P. A. Jaanimagi, *Bull. Am. Phys. Soc.* **29**, 1388, paper 8R8 (1984).
10. LLE Review **20**, 150 (1984).